Supplementary information

for

Deep blue thermally activated delayed fluorescence emitter: a balance between charge transfer and color purity

Bahadur Sk, Ezhaikudiyan Ravindran, Upasana Deori, Nisha Yadav, Gyana Prakash Nanda, Pachaiyappan Rajamalli,*

Materials Research Centre, Indian Institute of Science (IISc) Bangalore, C. V. Raman Road, Bengaluru, 560012, Karnataka, India

Email-rajamalli@iisc.ac.in

Contents

1. Materials and Methods

1.1 Chemicals:

All chemicals were used as received unless otherwise stated. The chemicals were received from Sigma-Aldrich, Merck India and Alfa aesar.

1.2 Instrumentation:

The ^{1}H and ^{13}C NMR spectra were recorded by using Bruker Avance 400 spectrometer. The HRMS were measured using MAT-95XL HRMS or MStation. The UV-visible absorption spectra were taken on a Hitachi U-3300 spectrophotometer. Fluorescence and phosphorescence spectra were recorded on a Hitachi F-7100 spectrophotometer. The absolute PL quantum efficiency of the doped films were determined using an integrating sphere under N_2 atmosphere. The time-resolved emission spectra and decays were recorded using an Edinburgh Instruments FLS980 spectrometer equipped with a double monochromator for both excitation and emission, operating in right-angle geometry mode and the highly sensitive photomultiplier tube (RED PMT in Cooled Housing) positioned after a double emission monochromator. Photoluminescence lifetime is measured the integrated device in Edinburgh instrument FLS980 model.

Thermal stability of 3BPy-*p*DTC was studied using TA Instruments Q50 TGA thermogravimetric analyser. The TGA curve which was recorded under N_2 flow from room temperature to 600 °C for 3BPy-*p*DTC exhibits thermal stability up to 450 °C. The cyclic voltammetry measurement was carried out in deoxygenated dichloromethane (DCM) with 0.1 M tetrabutylammonium hexafluorophosphate (TBAP) as supporting electrolyte in a three-electrode system using BioLogic SP200 potentiostat (BioLogic, France). Platinum (Pt) was used as a working electrode, platinum wire (Pt) and Ag/AgCl were used as counter and reference electrodes, respectively. The scan rate was kept at 100 mV/s for the measurement. The HOMO energy levels were determined from the onset of the oxidation potential using the equation $-(4.8\ eV + E_{ox}\ (vs\ Fc_{ox}))$.

2. Synthesis and Characterizations

2.1 Synthesis of (4-Bromophenyl)(6-bromopyridin-3-yl)methanone (3BPy)[1]

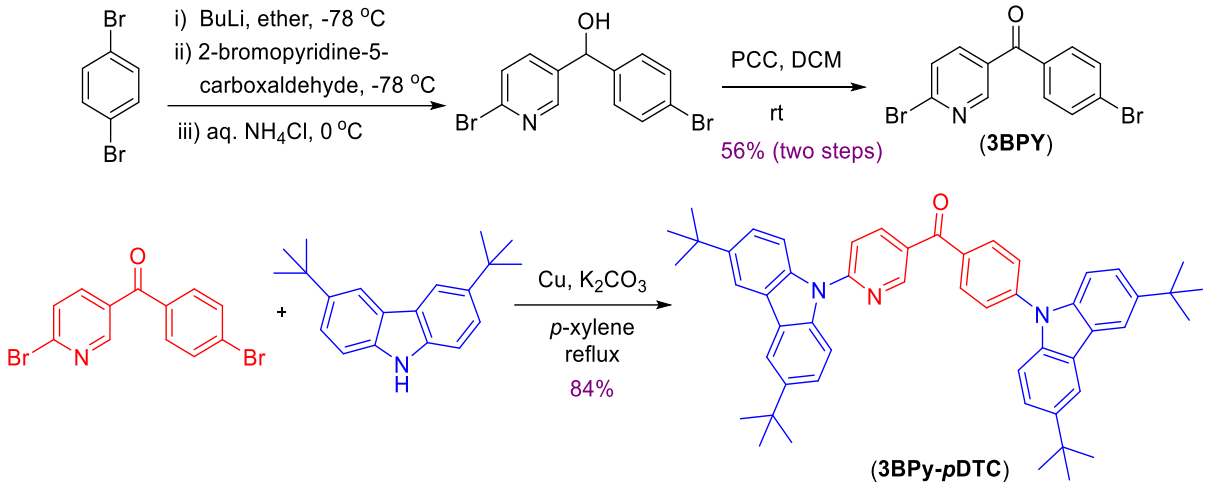

Scheme S1. Synthetic Scheme of (4-(3,6-di-*tert*-butyl-9*H*-carbazol-9-yl)phenyl)(6-(3,6-di-*tert*-butyl-9*H*-carbazol-9-yl)pyridin-3-yl)methanone (**3BPy-*p*DTC**).

To a stirred solution of 1,4-dibromobenzene (10.20 g, 43.24 mmol) in THF (100 mL) at -78 °C was added *n*-BuLi (8.65 mL, 21.62 mmol) and stirred for 30 minutes at the same temperature. To this solution, 2-bromopyridine-5-carboxaldehyde (4.00 g, 21.62 mmol) in THF (20 mL) was added drop wise and the reaction mixture was allowed to stir for another 2 h at -78 °C. It was quenched with aq. NH_4Cl at 0 °C and partitioned between water and DCM. The organic layer was washed with water and dried (Na_2SO_4). To this DCM layer was added pyridinium chlorochromate (10.91 g, 50.62 mmol) and stirred at room temperature for 4 h. The reaction mixture was filtered through celite pad and the celite pad was washed with DCM. Evaporation of solvent followed by column chromatographic purification gave **3BPy** in 56% (8.26 g) yield as colourless solid. **^{1}H NMR** (400 MHz, $CDCl_3$): δ 8.65 (s, 1 H), 8.68–8.67 (m, 1 H), 7.94–7.91 (m, 4 H), 7.63 (d, J = 9.6 Hz, 1 H).

2.2 Synthesis of (4-(3,6-di-*tert*-butyl-9*H*-carbazol-9-yl)phenyl)(6-(3,6-di-*tert*-butyl-9*H*-carbazol-9-yl)pyridin-3-yl)methanone (3BPy-*p*DTC)[1]:

An oven dried 100 mL double neck round bottom flask fitted with magnetic pallet and a rubber septum. To this round bottom flask (4-Bromophenyl)(6-bromopyridin-3-yl)methanone (**3BPy**) (2.0 g, 5.85 mmol), *t*-butyl carbazole (3.59 g, 11.70 mmol), Cu (0.74 g, 11.69 mmol) and K_2CO_3 (3.23 g, 23.40 mmol) were added. The system was evacuated and was purged with nitrogen. Then, *p*-xylene (20 mL) was added. The resulting reaction mixture was heated with stirring at 130 °C for 24 h. After completion of the reaction, the reaction mixture was filtered through the combination of celite and silica bed and washed with ethyl acetate (50

mL). The combined filtrate was evaporated under reduced pressure and the residue was purified by column chromatography using ethyl acetate/*n*-hexane as the eluent to afford 84% (3.64 g) of **3BPy-*p*DTC** in spectroscopically pure form. **^{1}H NMR** (400 M{Oda, 2019 #689}Hz, $CDCl_3$) δ 9.20 (dd, *J* = 2.4, 0.7 Hz, 1H), 8.45 (dd, *J* = 8.5, 2.4 Hz, 1H), 8.16 (d, *J* = 1.3 Hz, 3H), 8.14 (s, 1H), 8.12 (d, *J* = 2.0 Hz, 2H), 8.03 (d, *J* = 8.7 Hz, 2H), 7.86 (dd, *J* = 8.6, 0.8 Hz, 1H), 7.81 (d, *J* = 8.5 Hz, 2H), 7.56 (d, *J* = 2.0 Hz, 1H), 7.53 (d, *J* = 2.0 Hz, 1H), 7.52 (d, *J* = 1.3 Hz, 4H), 1.49 (d, *J* = 2.0 Hz, 36H). **^{13}C NMR** (101 MHz, $CDCl_3$) δ 192.88, 155.27, 151.63, 145.20, 143.95, 142.89, 139.82, 138.66, 137.59, 135.04, 131.85, 129.24, 126.09, 125.37, 124.36, 124.17, 124.08, 116.76, 116.60, 116.40, 111.87, 109.46, 34.95, 34.93, 32.12, 32.02. **HRMS (ESI) mass**: calculated for $C_{52}H_{55}N_3O$ is 738.4423 and found 738.4420.

3. Computational calculations and crystal structure

A time-dependent density functional theory (TDDFT, spin unrestricted) investigation for 3BPy-*p*DTC and 3BPy-*m*DTC were performed using the Gaussian 09 program package in the delta-cluster of SERC facility @IISc. The ground state molecular geometries of D-A compounds were optimized employing density functional theory (DFT) B3LYP hybrid functional and 6-311G(d,p) basis set in Gaussian 09 software.[2] The TDDFT calculations with the same functionality and the basis set was employed to obtain the excited-state structure. GaussView 5.0 and Chemcraft (version 1.8) were used to analyze the molecular orbitals. The iso values ±0.03 were used for the HOMO-LUMO orbital picture and ±0.001 for hole-electron distributions. The spatial distributions of the highest occupied molecular orbital (HOMO) and the lowest unoccupied molecular orbital (LUMO) of 3BPy-*p*DTC and 3BPy-*m*DTC in the ground and the excited state were analysed (Fig. 1). The hole and electron distribution were analysed using *Multiwfn* program package (Fig. S1).[3]

Table S1. The salient features of the most probable electronic transitions with oscillator strengths of 3BPy-*p*DTC and 3BPy-*m*DTC obtained from the TDDFT calculations at B3LYP/6-311G(d,p) level.

Compound	λ_{ex}	*f*	Transitions
3BPy-*p*DTC	426	0.481	HOMO to LUMO (93%)
	402	0.122	H-1 to LUMO (94%)
	331	0.068	H-1 to L+1 (81%), HOMO to L+1 (11%)
	322	0.014	HOMO to L+1 (66%), HOMO to L+2 (15%)
	320	0.071	HOMO to L+1 (13%), HOMO to L+2 (74%)
	312	0.028	H-1 to L+3 (82%), HOMO to L+3 (11%)
3BPy-*m*DTC	464	0.009	HOMO to LUMO (95%)
	453	0.009	H-1 to LUMO (95%)
	338	0.164	H-1 to L+1 (26%), HOMO to L+1 (54%)

	319	0.065	H-1 to L+2 (56%), H-1 to L+3 (12%), HOMO to L+4 (23%)
	314	0.075	H-1 to L+3 (65%), HOMO to L+3 (16%)

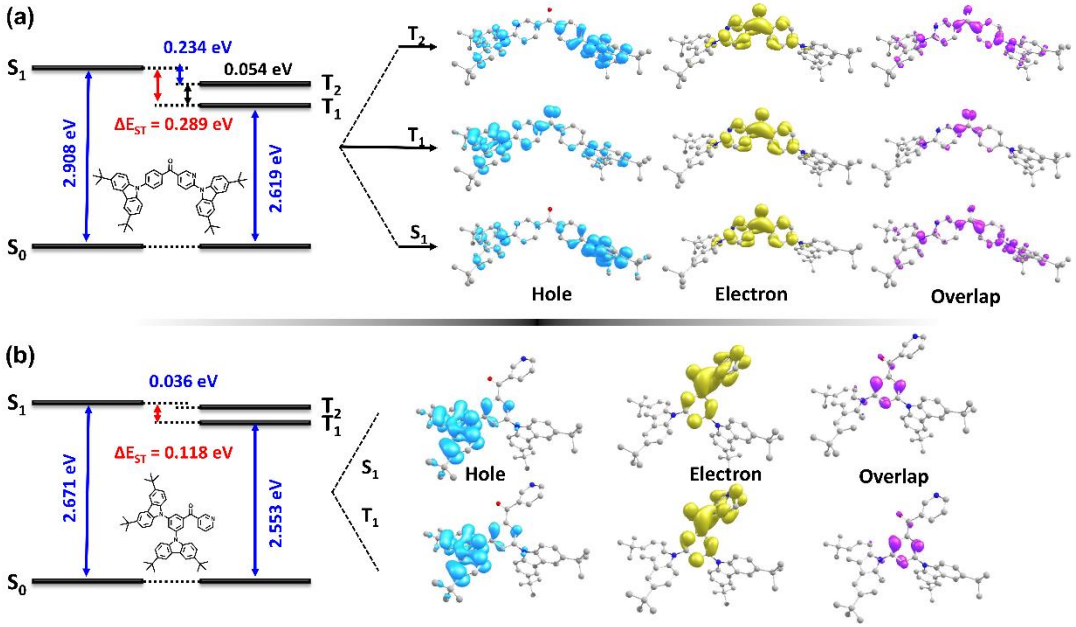

Fig. S1 A comparative TDDFT calculated energy profile diagram and the natural transition orbitals describing the excitation characters of the S_1, and T_1 states, the weights of the hole–electron contributions to the excitations of (a) 3BPy-*p*DTC and (b) 3BPy-*m*DTC are shown. (Isovalue = ±0.001)

Table S2. Summary of the computational and experimental outcome: Energy of first singlet (S_1), oscillator strength (f), energy of first triplet states (T_1), and energy gap between S_1 and T_1 (ΔE_{ST}) were calculated using DFT at the B3LYP/6-311g(d,p) level in vacuum; overlap integral between hole and electron were calculated using *Multiwfn*,[3] the experimental Stokes shift $\Delta\bar{\vartheta}$ (cm^{-1}), ΔE_{ST} measured in degassed 10 μM toluene.

Compound	**Substitution**	**$\Delta\bar{\vartheta}$ (cm^{-1})**	**S_1 (eV)**	***f***	**T_1 (eV)**	**$\Delta E_{ST}^{\#}$ (eV)**	**$\Delta E_{ST}^{\#\#}$ (eV)**	***FWHM (nm)**
3BPy-pDTC	*para*	2374	2.908	0.481	2.619	0.289	0.19	58
3BPy-mDTC	*meta*	5833	2.671	0.009	2.553	0.118	0.05	66

$^{\#}$Computed results, $^{\#\#}$Experimental results, *Electroluminescence spectra

Table S3. Crystal data table of 3BPy-*p*DTC.

Identification code	3BPy-*p*DTC
Empirical formula	C52 H55 N3 O
Formula weight	737.99
Temperature	100(2) K
Wavelength	1.54178 Å
Crystal system	Monoclinic

Space group	P 21/c
Unit cell dimensions	a = 23.1420(5) Å, α= 90° b = 16.9301(4) Å, β= 110.9490(10)° c = 23.0145(5) Å, γ = 90°
Volume	8421.0(3) $Å^3$
Z	8
Density (calculated)	1.164 Mg/m^3
Absorption coefficient	0.526 mm^{-1}
F(000)	3168
Crystal size	0.08 x 0.07 x 0.07 mm^3
Theta range for data collection	2.044 to 66.740°.
Index ranges	-27<=h<=25, -20<=k<=20, -16<=l<=27
Reflections collected	58072
Independent reflections	14766 [R(int) = 0.0336]
Completeness to theta = 67.679°	96.9 %
Absorption correction	Semi-empirical from equivalents
Max. and min. transmission	0.9492 and 0.8323
Refinement method	Full-matrix least-squares on F^2
Data / restraints / parameters	14766 / 126 / 1073
Goodness-of-fit on F^2	1.027
Final R indices [I>2sigma(I)]	R1 = 0.0517, wR2 = 0.1390
R indices (all data)	R1 = 0.0633, wR2 = 0.1487
Largest diff. peak and hole	0.666 and -0.507 $e.Å^{-3}$
CCDC number	**2116276**

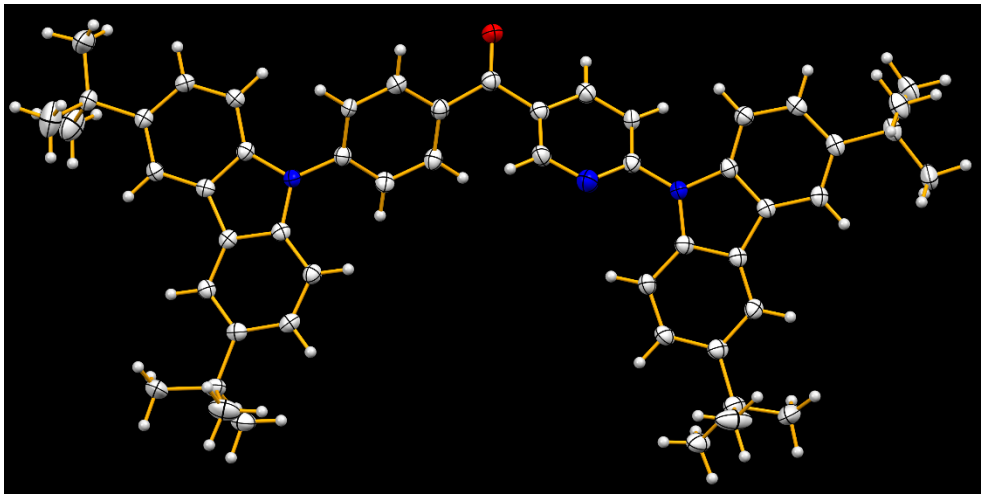

Fig. S2 ORTEP diagram of 3BPy-*p*DTC obtained from single crystal X-ray analysis shown with 50% ellipsoids.

4. Spectroscopic Characterizations

4.1 Electronic absorption:

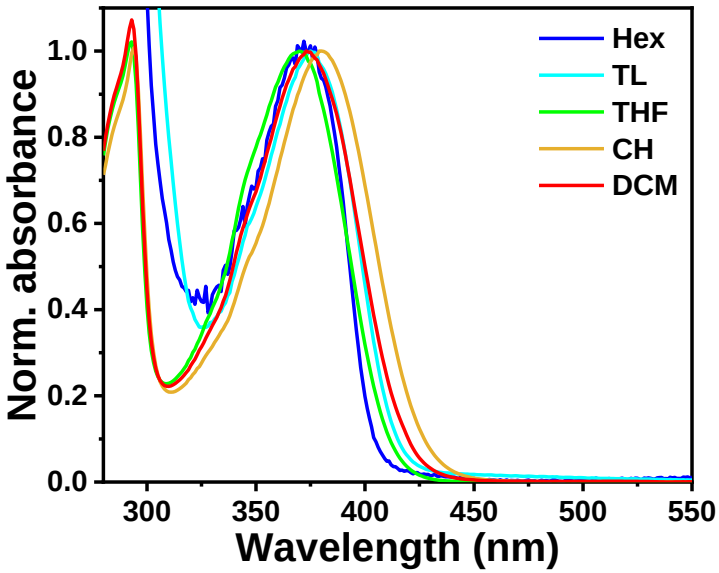

Fig. S3 Normalized absorption spectra of 3BPy-*p*DTC in different solvents with varying polarity. Hex: Hexane (0.009), TL: toluene (0.099), THF: tetrahydrofuran (0.207), CH: chloroform (0.259) and DCM: dichloromethane (0.309). The solvent polarity parameter (E_T^N value) is mentioned in the parenthesis.

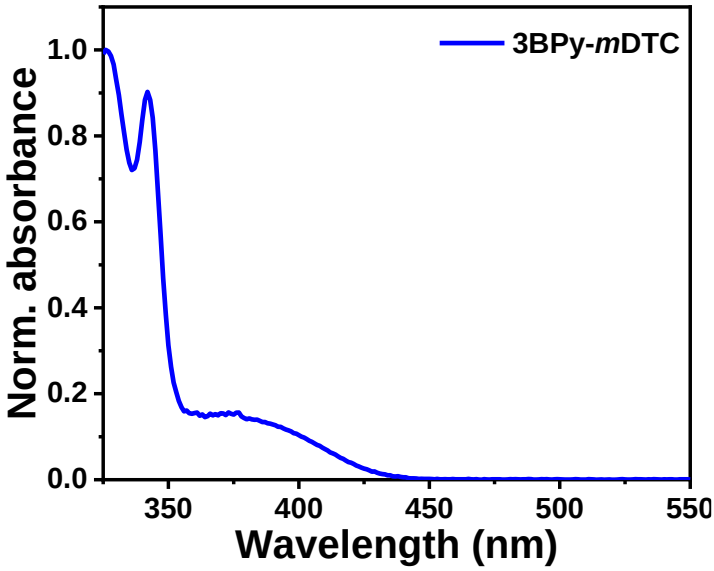

Fig. S4 Normalized absorption spectrum of 3BPy-*m*DTC in toluene at room temperature.

4.2 Emission spectroscopy:

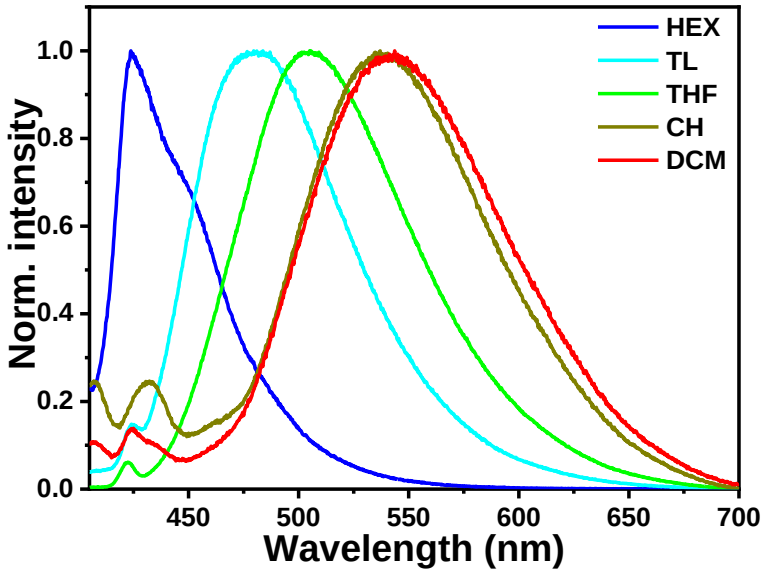

Fig. S5 Normalized emission spectra (λ_{ex} = 385 nm) of 3BPy-*m*DTC in different solvents with varying polarity. Hex: Hexane (0.009), TL: toluene (0.099), THF: tetrahydrofuran (0.207), CH: chloroform (0.259) and DCM: dichloromethane (0.309). The solvent polarity parameter (E_T^N value) is mentioned in the parenthesis.

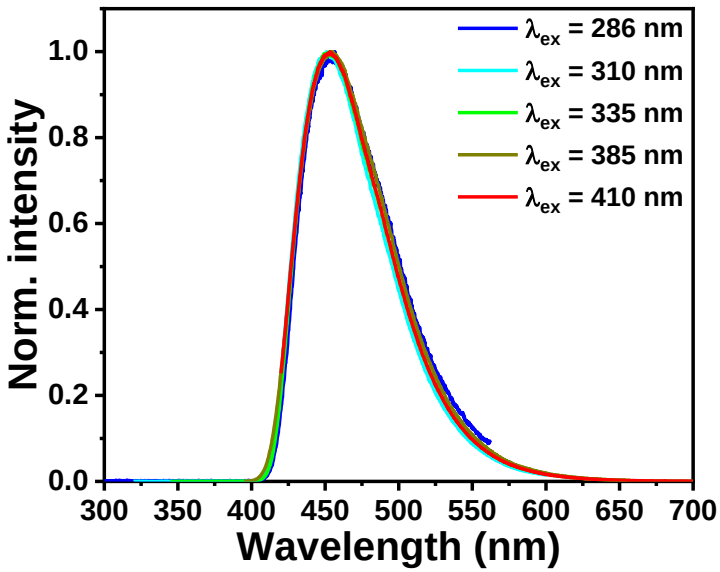

Fig. S6 Normalized emission spectra of 3BPy-*p*DTC in toluene at room temperature with different excitation wavelengths.

Table S4. Spectroscopic data table of 3BPy-*p*DTC

Solvent	E_T^N	Orientation polarizability (Δf)	λ_{abs} (nm)	λ_{em} (nm)	Stokes shift (nm)	Δυ (cm^{-1})	FWHM (nm)
HEX	0.009	0.0012	370	434	**64**	3986	66
TL	0.099	0.014	375	453	**78**	4591	73
THF	0.207	0.210	369	495	**126**	6898	97
CH	0.259	0.1488	374	512	**138**	7207	99
DCM	0.309	0.217	373	530	**157**	7941	108

Table S5. Spectroscopic data table of 3BPy-*m*DTC

Solvent	E_T^N	Orientation polarizability (Δf)	λ_{abs} (nm)	λ_{em} (nm)	Stokes shift (nm)	Δυ (cm^{-1})
HEX	0.009	0.0012	380	424	**44**	2731
TL	0.099	0.014	382	480	**98**	5345
THF	0.207	0.210	378	505	**127**	6654
CH	0.259	0.1488	380	538	**158**	7728
DCM	0.309	0.217	378	542	**164**	8005

4.3 Lippert-Mataga Equation:

Solvent-dependent shifts in the fluorescence maxima of the molecules can be mainly attributed to the dipole-dipole interactions between the fluorophore and solvent.[4, 5] Positive solvatochromism is observed when there is a redshift in emission with increasing the solvent polarity. This is because of the stabilized excited state. The Lippert-Mataga (L-M) theory describes the solvent dependence spectral shifts as given in Eq. 1.

$$\Delta\nu = \bar{\nu}_a - \bar{\nu}_f = \frac{2}{hc}\left(\frac{\varepsilon - 1}{2\varepsilon + 1} - \frac{n^2 - 1}{2n^2 + 1}\right)\frac{(\mu_E - \mu_G)^2}{a^3} + constant \quad \ldots. \ (1)$$

Where: $\bar{\nu}_a = \frac{1}{\lambda_{abs}^{max}}$, $\bar{\nu}_f = \frac{1}{\lambda_{em}^{max}}$ $\quad and \ \Delta f = \left(\frac{\varepsilon-1}{2\varepsilon+1} - \frac{n^2-1}{2n^2+1}\right)$ $\quad \ldots. \ (2)$

In this theory, specific solvent-fluorophore interactions, such as hydrogen bonding are not included. Eq. 1 shows Stokes shift ($\Delta\bar{\nu}$) depends on the dipole moments of the fluorophore in the ground (μ_G) and the excited (μ_E) state, respectively. It also depends on the dielectric constant (ε) and the refractive index (η) of the corresponding solvent. $\bar{\nu}_a$ and $\bar{\nu}_f$ represent the wavenumbers of the absorption and the fluorescence emission, respectively, *h* is the Planck's constant, *c* is the speed of light in vacuum, and *a* is the Onsager radius of the cavity in which the fluorophore resides. Δ*f* is the orientation polarizability of the solvent (Eq. 2). Plotting the Stokes shift as a function of the orientation polarizability of the solvents gives the Lippert-Mataga plot (Fig. S7-S8).

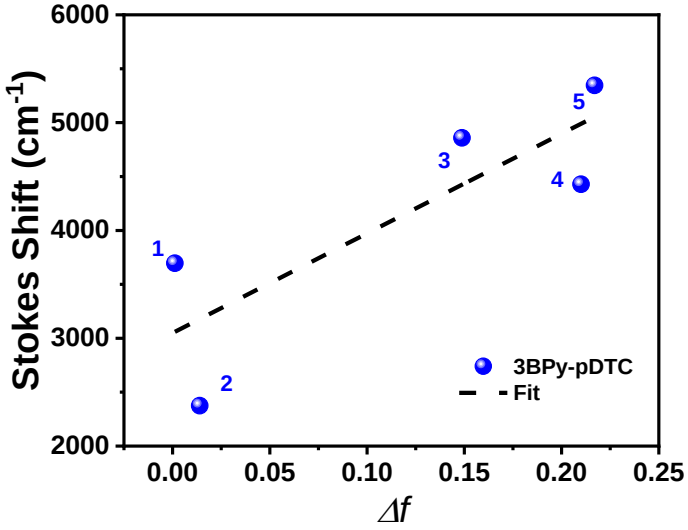

Fig. S7 Lippert-Mataga plot depicting Stokes shift ($\Delta\overline{\nu}$) versus the solvent orientation polarizability (Δf) of 3BPy-*p*DTC. The numbers refer to the solvents: (1) Hexane, (2) toluene, (3) tetrahydrofuran, (4) chloroform and (5) dichloromethane. The dashed line represents the best linear fit to the data points.

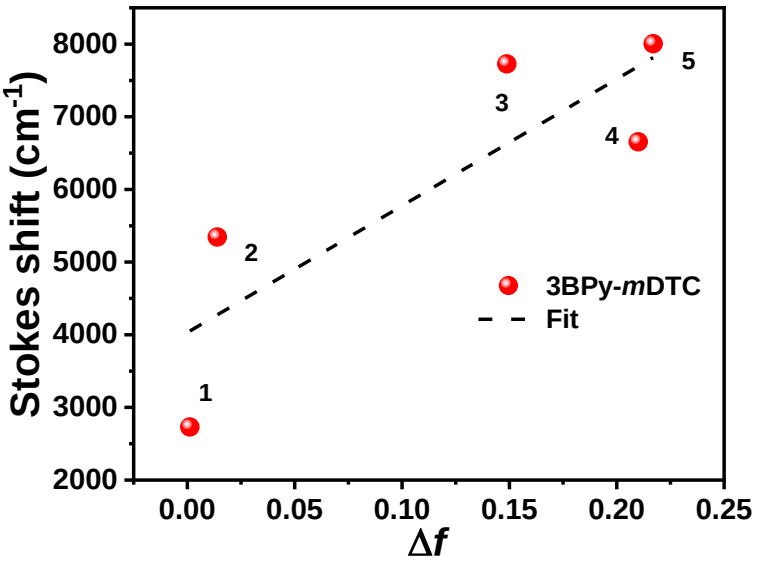

Fig. S8 Lippert-Mataga plot depicting Stokes shift ($\Delta\overline{\nu}$) versus the solvent orientation polarizability (Δf) of 3BPy-*m*DTC. The numbers refer to the solvents: (1) Hexane, (2) toluene, (3) tetrahydrofuran, (4) chloroform and (5) dichloromethane. The dashed line represents the best linear fit to the data points.

The change of the dipole moment (Δμ) can be estimated using the equation (1) from the slope obtained from the L-M plot as following

$$(\mu_E - \mu_G)^2 = \frac{Slope * (\mathrm{h}ca^3)}{2} \ldots. \quad (3)$$

Δ μ(μ_E - μ_G) is the change of dipole moment from the ground to an excited state.

Table S6 Fitting parameters of Lippert-Mataga plots and calculated Onsager radius (a), Δμ (μ_E - μ_G) refers the change in dipole moment. (R^2: goodness of fit)

Compound	Slope (cm^{-1})	R^2	a (Å)[#]	(μ_E - μ_G) D
3BPy-*p*DTC	15882	0.92	6.61	**21**
3BPy-*m*DTC	17442	0.72	7.30	**26**

[#]The Onsager radius can be calculated from the geometry optimized structure of the compounds using DFT minimization in Gaussian program (B3LYP functional using 6-31G-(d) orbital base.[6]

4.4 Fluorescence quantum yield measurement:

The photoluminescence quantum yield (PLQY) of 3BPy-*p*DTC was estimated by comparison with 9,10-diphenylanthracene dye in toluene (Φ_f = 0.95).[7, 8]

$$\Phi_{f,x} = \Phi_{f,s} \times \frac{F_X}{F_S} \times \frac{f_S}{f_X} \times \frac{n_X^2}{n_S^2} \ldots. \quad (4)$$

Where Φ_f is the fluorescence quantum yield, the subscript x denotes sample, and the subscript s refers to the standard dye. F denotes integral fluorescence, n refers to the refractive index of the solvent used in the measurements and f is the absorption factor at the excitation wavelength given by the following equation: $f = 1 - 10^{-\varepsilon(\lambda_{ex})cl} = 1 - 10^{-A(\lambda_{ex})}$, where A is the absorbance, and ε = molar extinction coefficient in L mol^{-1} cm^{-1}.

4.5 Time-resolved spectroscopy:

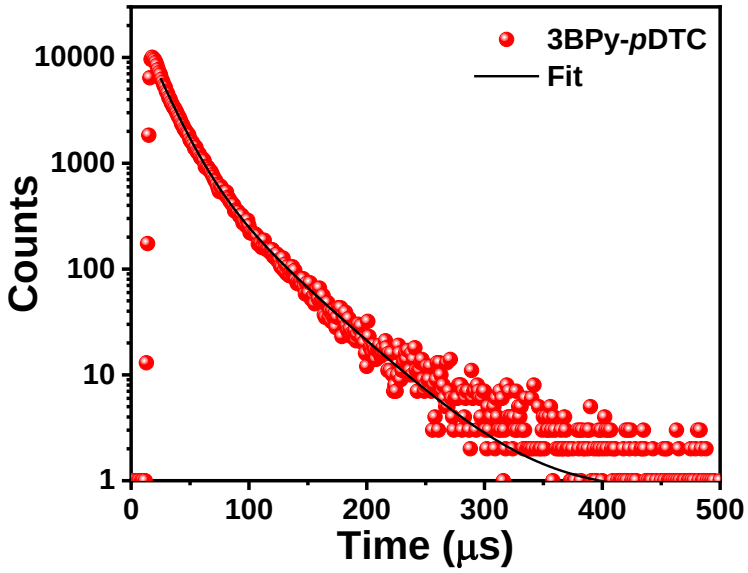

Fig. S9. Emission decay profile of 3BPy-*p*DTC (λ_{ex} = 375 nm, λ_{em} = 470 nm) film doped in PMMA matrix at room temperature.

Table S7. Emission decay parameters (λ_{ex}= 375 nm, λ_{em}= 450 nm) of 3BPy-*p*DTC in toluene (TL), 10 wt% PMMA film at room temperature; the decay times (τ_1, and τ_2), the respective fractional contributions (α_1, and α_2 mentioned in parentheses), the weighted average decay time ($\tau_{avg.}$) and the quality of fitting ($\chi 2$) are shown.

Sample	Timescales	τ_1	α_1	τ_2	α_2	$\tau_{avg.}$	$\chi 2$
TL	ns	0.8	69	3.2	31	1.5	1.18
	μs	5.2	77	16.2	23	7.73	1.24
PMMA	μs	15.9	64	43.7	36	25.9	1.00

5. Electrochemical measurement

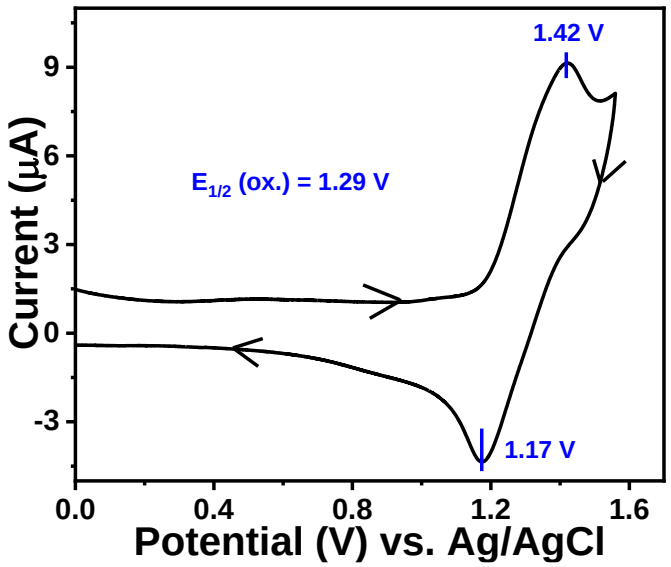

Fig. S10. Cyclic voltammogram (100 mV/s) of 3BPy-*p*DTC in dry dichloromethane (1 mM solution) using 0.1 M tetrabutylammonium hexafluorophosphate (TBAP) as supporting electrolyte and Pt as the working electrode and Ag/AgCl as a reference electrode.

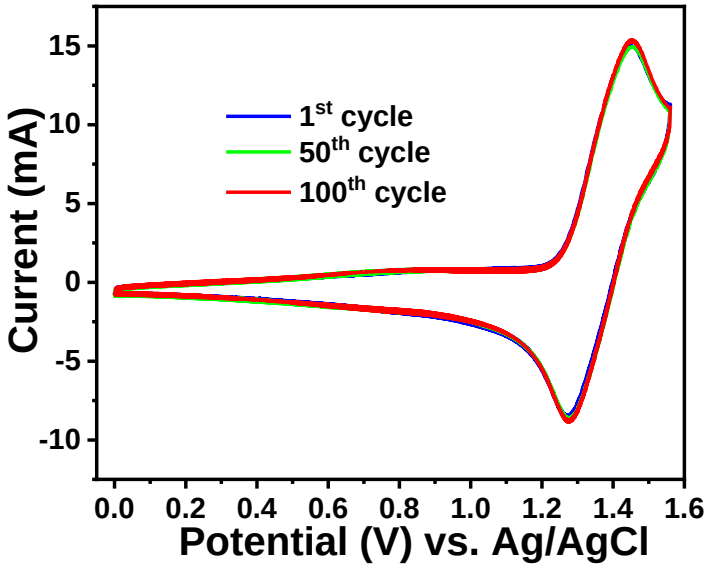

Fig. S11 Electrochemical stability of 3BPy-*p*DTC in DCM up to 100 cycles at a scan rate of 100 mV/s vs. Ag/AgCl.

6. Thermal stability and photostability

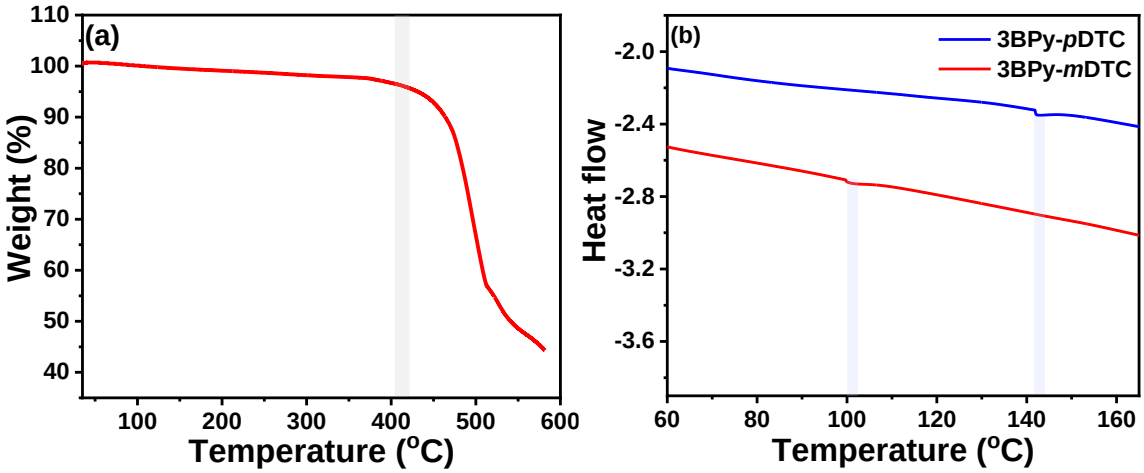

Fig. S12 (a) Thermogravimetric analysis (TGA) graph of 3BPy-*p*DTC in nitrogen atmosphere and (b) differential scanning calorimetry (DSC) graphs of 3BPy-*p*DTC and 3BPy-*m*DTC.

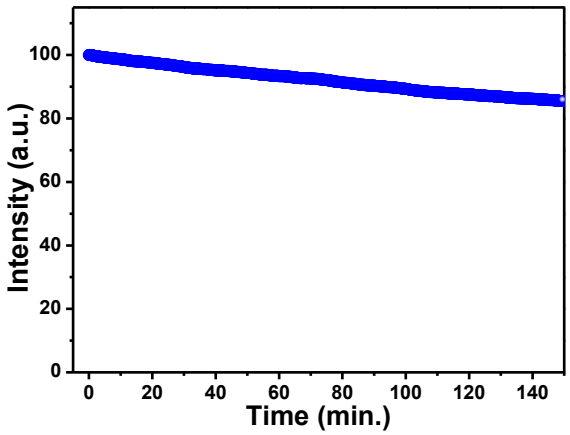

Fig. S13 The fluorescence intensity profile of 3BPy-*p*DTC film doped in PMMA matrix ($\lambda_{ex.}$ = 375 and $\lambda_{em.}$ = 455 nm) with time. The continuous irradiation of 150 W xenon lamp for over 2.5 hours depicting the photostability.

7. Device Fabrication

The organic materials used for the OLED device fabrication were purified by sublimation. Devices were fabricated by vacuum deposition onto pre-coated ITO glass with sheet resistance of 15 Ω/square at a pressure lower than 10^{-6} Torr. The organic materials were deposited at the rate of 0.5~1.2 Å s^{-1}. LiF and Al were deposited at the rate of 0.1 Å s^{-1}, 3-10 Å s^{-1}, respectively. The rest of the procedures are similar to the reported method.[1, 9, 10]

The transient electroluminescence measurements were carried out on a function generator (Agilent 8114A) and an indigenously developed time-resolved emission spectrometer. The devices were driven by a voltage pulse 6 V with a repetition rate of 20 kHz and pulse width of 10 μs. The emission decay curves at specific wavelengths were gained using a cooled photomultiplier tube (PMT) detector (Becker & Hickl GmbH PMC-100) integrated with a 300 nm focal length monochromator (Princeton Instruments Acton SP2300). The time-resolved photon counting was done via a multichannel scaling (MCS) card (Becker & Hickl GmbH MSA-300) with a time resolution of 5 ns. The whole system was synchronized with a digital delay generator (Stanford Research Systems DG645).

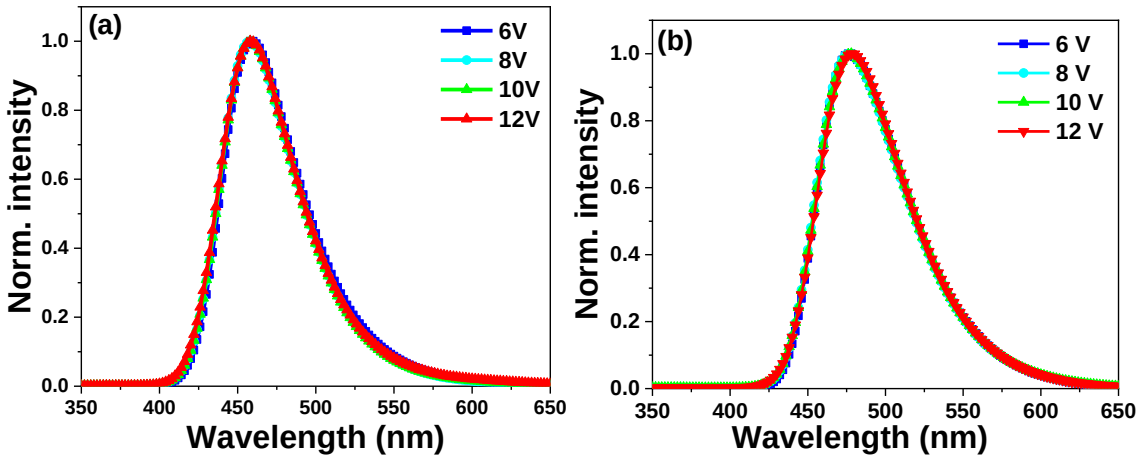

Fig. S14 Normalized electroluminescence spectra of (a) 3BPy-*p*DTC and (b) 3BPy-*m*DTC with varying voltages depicting the stability and colour purity.

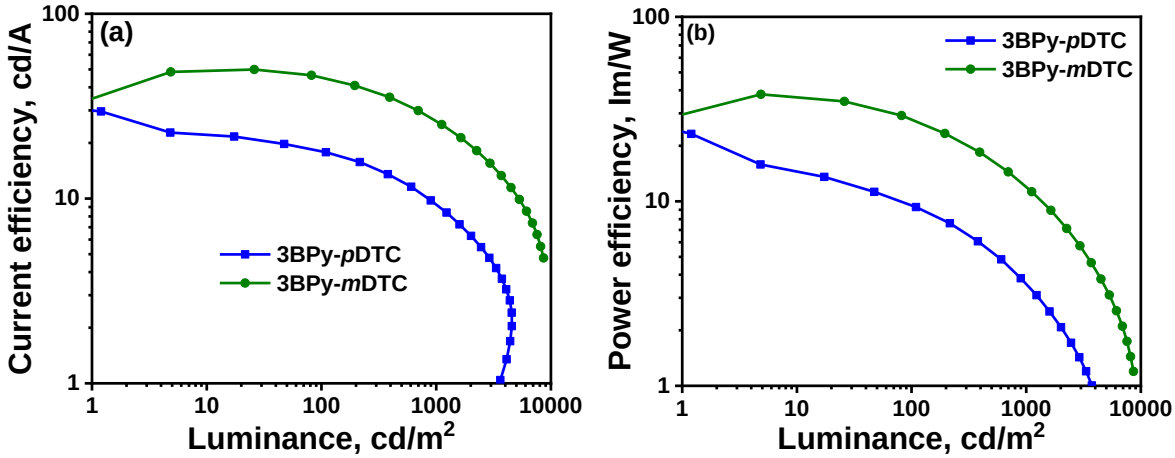

Fig. S15 (a) The current efficiency vs luminance, (b) power efficiency vs luminance of 3BPy-*p*DTC and 3BPy-*m*DTC devices.

Table S8. A comparative table for the blue TADF and MR-TADF emitters with CIEy is ≤0.15.

Nature of Emitters	Molecules	λ_{em} (nm, eV)	FWHM (nm, eV)	CIE	EQE_{max} (%)	Citation
TADF	**3BPy-*p*DTC**	**458**	**58**	**(0.14, 0.13)**	**25%**	**This work**
TADF	ICz-DPS	435	NR	(0.15, 0.08)	11.7%	*ACS Appl. Mater. Interfaces* **2021**, DOI: 10.1021/acsami.1c17449
TADF	tBuPCAPICN	452	53	(0.15, 0.11)	12.7%	*CCS Chem.*, **2020**, *2*, 2557
TADF	TDBA-SBA	467	55	(0.13, 0.15)	29.3%	*Chem. Eng. J.*, **2021**, DOI: 10.1016/j.cej.2021.133598
TADF	HAP-3DPA	440	NR	(0.16, 0.13)	12.5%	*Photonics* **2021**, *8*, 293. https://doi.org/10.3390/photonics8080293

TADF	BNNIO	415	NR	(0.150, 0.076)	-	*J. Phys. Chem. Lett.* **2021**, *12*, 9501
TADF	OBO-I	457	60	(0.14, 0.10)	21.7%	*Adv. Optical Mater.* **2021**, 2101282
TADF/ HyperFlu	DBA–BFICz/ DBA–BTICz	476/ 473	64/19	(0.15, 0.24)/ (0.12, 0.15)	33.2/38.8 %	*Adv. Funct. Mater.* **2021**, *31*, 2105805
TADF	sAC-sDBB	452	51	(0.155, 0.089)	22.5	*Angew.Chem. Int. Ed.* **2021**, *60*,9598
TADF	TDBA-SAF	456	55	(0.142, 0.090)	28.2	*Adv. Mater.* **2020**, *32*, 2004083
TADF	TDBA–Ac	-	48	(0.15, 0.06)	21.5%	*Nat. Photonics*, **2019**, *13*, 540
TADF	BFCZPZ1	436	59	(0.15, 0.06)	6.5%	*Chem. Eng. J.* **2021**, *doi.org/10.1016/j.cej.2020.127591*
TADF	2CzBN	433	70	(0.15, 0.07)	11.4	*Chem. Eng. J.* **2021**, *416*, 129097
TADF	DMACpB	471	NR	(0.138, 0.142)	20%	*Dyes Pigm.* **2021**, *188*, 109224
TADF	PXZN-B DMACN-B	468 444	48 44	(0.13, 0.147/ (0.15, 0.045)	12.7% 10%	*Adv. Funct. Mater.* **2021**, *31*, 2009488
TADF	DPFCz-TRZ	445	65	(0.15, 0.10)	15%	*ChemPhotoChem* **2020**, *4*, 321
TADF	TXADO-spiro-DMACF	444	54 (neat film)	(0.16, 0.09)	5.3%	*ACS Omega* **2019**, *4*, 1861
TADF	DMAC2PTO	448	50	(0.154, 0.108)	15.2%	*Dyes Pigm.* **2020**, *178*, 108367
TADF	DtBuAc-DBT	455	84	(0.133, 0.129)	10.5%	*J. Mater. Chem. C* **2019**, *7*, 13224
TADF	pDTCz-3DPyS	452	NR	(0.15, 0.13)	13.4%	*J. Mater. Chem. C* **2019**, *7*, 6664
TADF	PXB-mIC	438 (PL)	NR	(0.15, 0.08)	12.5%	*ACS Appl. Mater. Interfaces* **2019**, *11*, 14909
TADF	TXAZ	456	69	(0.148, 0.131)	16%	*ACS Appl. Mater. Interfaces* **2019**, *11*, 7199
TADF	CNICCz/ CNICtCz	449/ 456	56/ 60	(0.15, 0.08)/ (0.14, 0.13)	12.4%/ 16.0%	*J. Mater. Chem. C* **2018**, *6*, 5012
TADF	CzOMeoB	449	NR	(0.151, 0.058)	14.9%	*Adv. Optical Mater.* **2018**, *6*, 1800385
TADF	FA–TA	NR	NR	(0.15, 0.13)	11.2%	*Adv. Mater.* **2018**, *30*, 1705641
TADF	DCzBN3	428	65	(0.156, 0.063)	10.3%	*Adv. Funct. Mater.* **2018**, *28*, 1706023
TADF	Ac-3MHPM	451	NR	(0.16, 0.15)	17.8%	*ACS Appl. Mater. Interfaces* **2017**, *9*, 4742
TADF	CzoB	466	NR	(0.139, 0.150)	22.6%	*ACS Appl. Mater. Interfaces* **2017**, *9*, 24035
TADF	Cz-TRZ3	435 (TL)	NR	(0.14, 0.098)	19.2%	*Angew. Chem. Int. Ed.* **2017**, *56*, 1571
TADF	ICzAc	454	56	(0.15, 0.09)	13.7%	*ACS Appl. Mater. Interfaces* **2017**, *9*,

						37864
TADF	PX-SBA	448	NR	(0.16, 0.13)	17.8%	*Chem. Mater.* **2017**, *29*, 8630
TADF	acridan–pyrimidine (5)	458	NR	(0.15, 0.15)	11.4%	*Chem. Sci.*, **2017**, *8*, 953
TADF	CzBPCN	460	48	(0.14, 0.12)	14%	*Chem. Mater.* **2016**, *28*, 5400
TADF	DCzTrz	2.89 eV	NR	(0.15, 0.14)	16.6%	*Adv. Mater.* **2015**, *27*, 2515
MR-TADF	tDPAC-BN	440	19	(0.135, 0.094)	21.6%	*Chem. Eng. J.*, **2021**, https://doi.org/10.1016/j.cej.2021.133221
MR-TADF	QA-1/ QA-2	455/ 463	49/ 37	(0.14, 0.12)/ 0.13, 0.14	17.1%/ 19.0%	*Angew. Chem. Int. Ed.* **2021**, *60*, 7643
MR-TADF	DABNA-NP-TB	457	33	(0.14, 0.11)	19.5%	*Angew. Chem. Int. Ed.* **2021**, *60*, 2882
MR-TADF	t-DABNA		31	(0.13, 0.15)	31.4%	*J. Mater. Chem. C* **2019**, *7*, 3082
MR-TADF	B2	460	37	(0.13, 0.11)	18.3%	*J. Am. Chem. Soc.* **2018**, *140*, 1195
MR-TADF	DABNA-2	467	28	(0.12, 0.13)	20.2%	*Adv. Mater.* **2016**, *28*, 2777
MR-TADF	ν-DABNA	469	18	(0.12, 0.11)	34.4%	*Nat. Photonics* **2019**, *13*, 678

NR = not reported

8. References

1. P. Rajamalli, V. Thangaraji, N. Senthilkumar, C.-C. Ren-Wu, H.-W. Lin and C.-H. Cheng, *J. Mater. Chem. C*, 2017, **5**, 2919-2926.
2. M. J. Frisch, G. W. Trucks, H. B. Schlegel, G. E. Scuseria, M. A. Robb, J. R. Cheeseman, G. Scalmani, V. Barone, G. A. Petersson, H. Nakatsuji, X. Li, M. Caricato, A. V. Marenich, J. Bloino, B. G. Janesko, R. Gomperts, B. Mennucci, H. P. Hratchian, J. V. Ortiz, A. F. Izmaylov, J. L. Sonnenberg, Williams, F. Ding, F. Lipparini, F. Egidi, J. Goings, B. Peng, A. Petrone, T. Henderson, D. Ranasinghe, V. G. Zakrzewski, J. Gao, N. Rega, G. Zheng, W. Liang, M. Hada, M. Ehara, K. Toyota, R. Fukuda, J. Hasegawa, M. Ishida, T. Nakajima, Y. Honda, O. Kitao, H. Nakai, T. Vreven, K. Throssell, J. A. Montgomery Jr., J. E. Peralta, F. Ogliaro, M. J. Bearpark, J. J. Heyd, E. N. Brothers, K. N. Kudin, V. N. Staroverov, T. A. Keith, R. Kobayashi, J. Normand, K. Raghavachari, A. P. Rendell, J. C. Burant, S. S. Iyengar, J. Tomasi, M. Cossi, J. M. Millam, M. Klene, C. Adamo, R. Cammi, J. W. Ochterski, R. L. Martin, K. Morokuma, O. Farkas, J. B. Foresman and D. J. Fox, *Gaussian 09*, Gaussian, Inc., Wallingford CT, 2016.
3. T. Lu and F. Chen, *J. Comput. Chem.*, 2012, **33**, 580-592.
4. J. R. Lakowicz, *Principles of fluorescence spectroscopy*, Springer, New York, 2006.
5. B. Sk, S. Khodia and A. Patra, *Chem. Commun.*, 2018, **54**, 1786-1789.
6. S. Mukherjee, A. Chattopadhyay, A. Samanta and T. Soujanya, *J. Phys. Chem.*, 1994, **98**, 2809-2812.
7. K. Rurack and M. Spieles, *Anal. Chem.*, 2011, **83**, 1232-1242.
8. C. Wurth, M. Grabolle, J. Pauli, M. Spieles and U. Resch-Genger, *Nat. Protoc.*, 2013, **8**, 1535-1550.
9. J.-J. Lin, W.-S. Liao, H.-J. Huang, F.-I. Wu and C.-H. Cheng, *Adv. Funct. Mater.*, 2008, **18**, 485-491.
10. P. Rajamalli, N. Senthilkumar, P. Gandeepan, P.-Y. Huang, M.-J. Huang, C.-Z. Ren-Wu, C.-Y. Yang, M.-J. Chiu, L.-K. Chu, H.-W. Lin and C.-H. Cheng, *J. Am. Chem. Soc.*, 2016, **138**, 628-634.

9. NMR Spectra

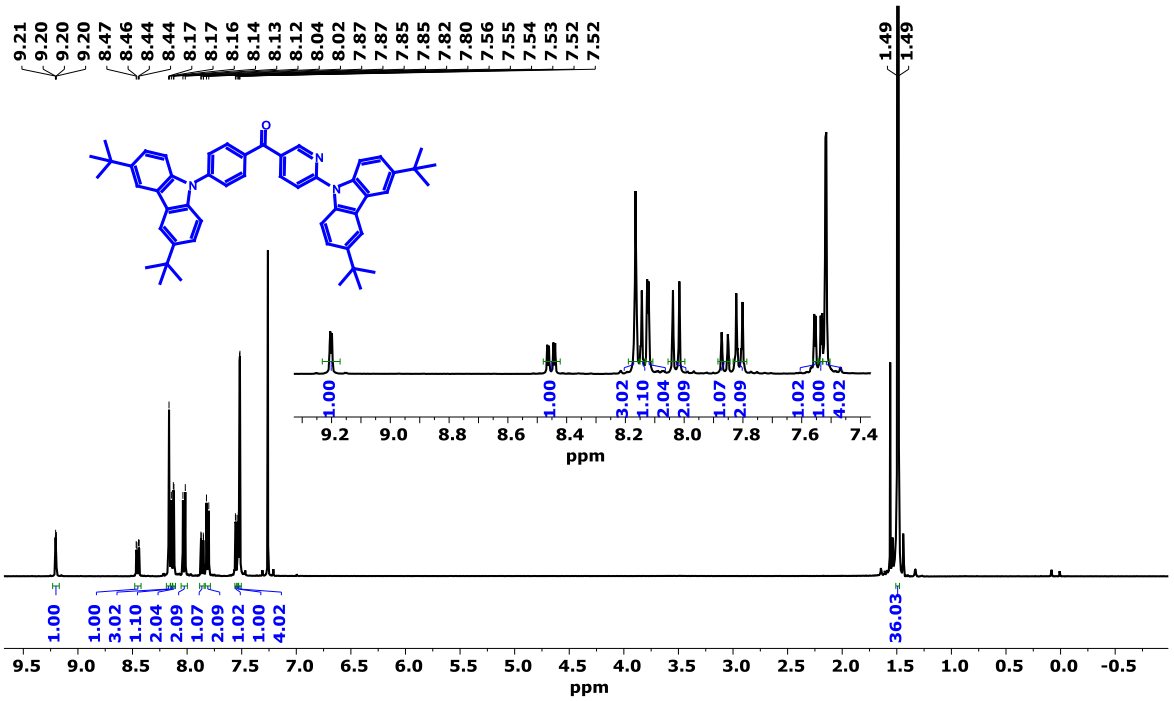

Fig. S16 ^{1}H NMR spectrum of (4-(3,6-di-*tert*-butyl-9*H*-carbazol-9-yl)phenyl)(6-(3,6-di-*tert*-butyl-9*H*-carbazol-9-yl)pyridin-3-yl)methanone (**3BPy-*p*DTC**) in $CDCl_3$.

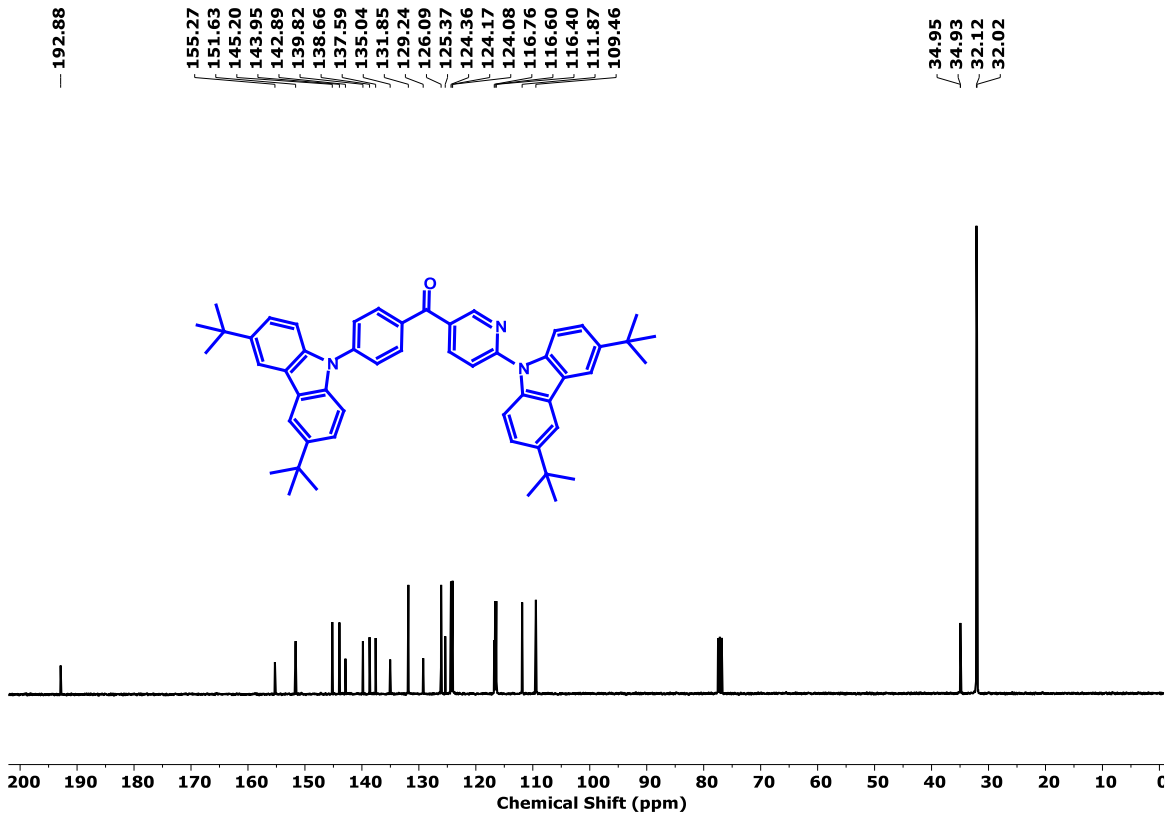

Fig. S17 ^{13}C NMR spectrum of (4-(3,6-di-*tert*-butyl-9*H*-carbazol-9-yl)phenyl)(6-(3,6-di-*tert*-butyl-9*H*-carbazol-9-yl)pyridin-3-yl)methanone (**3BPy-*p*DTC**) in $CDCl_3$.